Available online at www.sciencedirect.com
SCIENCE DIRECT®
Surface & Coatings Technology 201 (2006) 452–457
SURFACE & COATINGS TECHNOLOGY
www.elsevier.com/locate/surfcoat

Influence of the process temperature on the steel microstructure and hardening in pulsed plasma nitriding

L.F. Zagonel [a], C.A. Figueroa [a], R. Droppa Jr. [a,b], F. Alvarez [a,*]

[a] *Instituto de Física "Gleb Wataghin", Universidade Estadual de Campinas, 13083-970, Campinas, São Paulo, Brazil*
[b] *Laboratório Nacional de Luz Síncrotron, CP 6192 13084-971, Campinas, São Paulo, Brazil*

Received 7 May 2005; accepted in revised form 28 November 2005
Available online 31 January 2006

Abstract

In this paper we report the influence of temperature (260 to 510 °C) on the AISI H13 steel microstructure and hardness in pulsed plasma nitriding processes. The experimental results show that bulk nitrogen penetration is well represented by a temperature-activated law. Even at the lowest studied temperatures, grain boundary diffusion causes nitrogen to move relatively deep in the bulk sample. The microstructure was studied by X-ray diffraction analysis at grazing angle and in the Bragg–Brentano configuration. Scanning Electron Microscopy with spatially resolved X-ray energy disperse spectroscopy was also employed to map nitrogen influence on the morphology of the material. Also, surface (frontal) and profiling nano-indentation was utilized to elucidate the effect of the temperature on the nitrited material hardness.

PACS: 81.65.Lp; 81.30.Mh; 68.37.Hk
Keywords: Pulsed plasma nitriding; Tool steel; Diffusion mechanism; Microstructure

1. Introduction

Since the beginning of the last century, nitriding processes proved to be an important surface treatment. Thereafter, in the attempt to satisfy different industrial demands where fine nitriding control is required, several plasma techniques were developed [1,2]. All these techniques aim to produce a material surface with improved mechanical properties such as wear [3] and corrosion resistance and also to support a subsequent coating [4]. Depending on the process parameters, it is possible to obtain quite different mechanical properties, resulting in all sorts of results on a production line. For this reason, a full understanding of the thermo-chemical diffusion mechanism of nitrogen through the polycrystalline heterogeneous material (steel) is mandatory. Among the parameters controlling nitrogen diffusion, temperature is no doubt the most important one. The correct choice of temperature will give the best mechanical properties as well as determining minimum process time, an important economic factor.

In this paper we report a comprehensive study of the influence of temperature on the microstructure of nitrided hot work tool steel (AISI H13) and its influence on the material hardness. As it is well known, the influence of temperature is crucial on the nitrogen diffusion mechanism. The effect of temperature on nitrides precipitates is presented and the effect on nitrogen diffusion discussed.

The studied samples were treated at different temperatures, from 260 to 510 °C. This temperature range produces from very thin and hard up to very thick nitrided layers, without core hardness losses. As previously reported, diffusion studies [5] at a relative low temperature have been shown to give physical insight of the nitriding process applied to pure iron [6], low carbon steel [5], low alloy steel [7], and stainless steel [8–11]. As it is well known, also, the samples' microstructure and hardness values of the compound and diffusion layers depend on the temperature of the process. As remarked in other researches, the nitrogen concentration profiles also depend on the material characteristics. Finally, some mechanical,

* Corresponding author. Tel.: +55 19 37885372; fax: +55 19 37885376.
E-mail address: alvarez@ifi.unicamp.br (F. Alvarez).

0257-8972/$ - see front matter © 2005 Elsevier B.V. All rights reserved.
doi:10.1016/j.surfcoat.2005.11.137

Table 1
AISI H13 steel composition, weight percent

Element	Fe	C	Mn	Si	Cr	Mo	V
Content (wt.%)	Rest	0.6	0.4	1.1	5.7	1.3	1.0

crystalline, and morphological properties can be used to provide information about the diffusion process and nitrogen profiles [12–15].

2. Experimental

AISI H13 samples (2×15×20 mm) from a single lot were mirror polished and cleaned using standard metallographic techniques. The samples were heat treated by quenching in air from 1025 °C and tempering at 580 °C, presenting a bulk hardness of 7.5±0.4 GPa. Table 1 displays the material composition as determined by in situ photoemission electron spectroscopy (XPS) after sputtering cleaning (Ar^+, 10 min, 600 eV). The studied samples were treated at temperatures varying between 260 up to 510 °C. The process was performed in a commercial hot-wall fully automatic Plasmatec180 pulsed plasma system, 60 A/1000 V of maximum capacity (Plasma-LIITS, 13083-970 Campinas, São Paulo, Brazil). The plasma is generated by a pulsed DC power supply operating at 7.1 A and 380 V for all the studied samples. The temperature is reached by auxiliary heating and controlled by a thermocouples attached to the sample holder. During the process 70%H_2–30%N_2 gas mixture was used at 400 Pa fixed pressure. Before nitriding and for cleaning purposes, samples were ion bombarded during 4 h in plasma constituted by 80%Ar–20%H_2. After 5 h nitriding treatment, the samples were slowly cooled (~6 h) in vacuum up to room temperature.

Hardness measurements were performed on a commercial nano-indentation apparatus (NanoTest-300) with a Berkovich diamond tip. Load–displacement curves were analyzed with the Oliver and Pharr method [16,17]. Shallow indentations measurements were obtained normally to the nitrided surface sample. In this mode, the apparatus can prove hardness up to 1.5 μm depth. Also, a depth bulk hardness profile from 20 up to 400 μm was also performed. The reported hardness is the averaged value of ten indentations. Cross-section samples were prepared by cutting a slice from the original sample and mirror polishing the exposed surface. The X-ray diffractograms were obtained using a copper tube source in the Bragg–Brentano geometry with monochromatized radiation (Cu K_α, λ=0.15418 nm). Grazing-incident (0.5°, λ=0.15385 nm) X-ray diffraction (GID) experiments were performed at the XRD1 beamline, Laboratório Nacional de Luz Síncrotron (LNLS), Campinas, São Paulo, Brazil. The microstructure of the samples was analyzed using a scanning electron microscope (SEM) (Jeol JMS-5900LV), equipped with energy dispersive spectrometry (EDS). The samples for SEM studies were the same mirror-polished specimens used for in-depth hardness profiling. In order to expose the microstructure, the samples were etched for 5 s in a ~10% nital solution and immediately rinsed in analytical alcohol with the purpose of stopping the reaction.

3. Results and discussion

3.1. Profiling hardness

Figs. 1 and 2(a) and (b) represent the hardness profile for samples treated at different temperatures. As was previously reported, the hardness in-depth profiling scales fairly well with the nitrogen concentration in the material [12–15]. As observed, increasing process temperature causes increasing hardness, i.e., increasing nitrogen incorporation. However, it is interesting to note that, even at 260 °C, a sizable hardness increment is observed for large depths (Fig. 1). The hardness increase reaches a depth of up to ~100 μm for all nitrided samples treated at temperatures > 330 °C. These results suggest a quite efficient nitrogen diffusion process even at the relative low temperatures used in the experiments [7].

The pronounced hardness gradient observed in Fig. 2(a) is due to the relatively low temperature of the process. Indeed, nitrogen accumulates on the top of the layer due to the inefficient low temperature diffusion. Fig. 2(b), on the other hand, shows a smaller hardness gradient, due to the higher temperature nitriding process. Finally, the relatively high hardness values obtained at the surface suggest the presence of the ε-phase (hcp, $Fe_{2-3}N$) at the uppermost sample layers even in samples obtained at the lower studied process temperature [18,19]. Indeed, as shown in the next section, GID confirms the existence of this phase.

3.2. Crystallographic properties of the nitride layer

Fig. 3(a) and (b) shows the evolution of the diffraction peaks of the studied samples using the Bragg–Brentano and GID geometries, respectively. From the diffractograms obtained using the Bragg–Brentano geometry, the nitrided sample at ~260 °C shows only the original α (bcc) phase of the material (Fig. 3(a)). A higher process temperature (330 °C) induces the formation of an incipient ε-phase (hcp, $Fe_{2-3}N$) [20–23]. Further process temperature increments (370 and 420 °C) consolidate the presence of this phase in the material. At higher

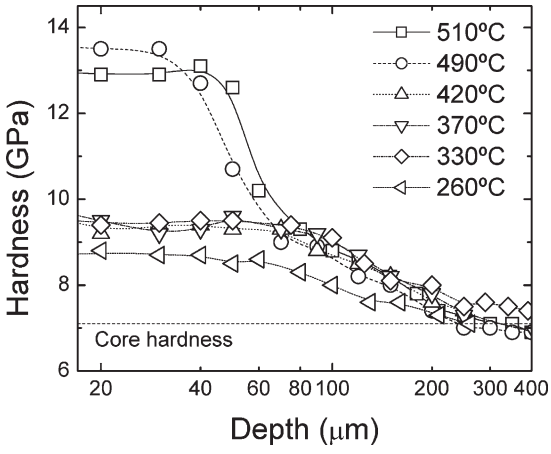

Fig. 1. In-depth hardness profile for several process temperatures. The error bars are of the order of the symbols' sizes. All curves merge at the nucleus hardness above ~200–300 μm depth.

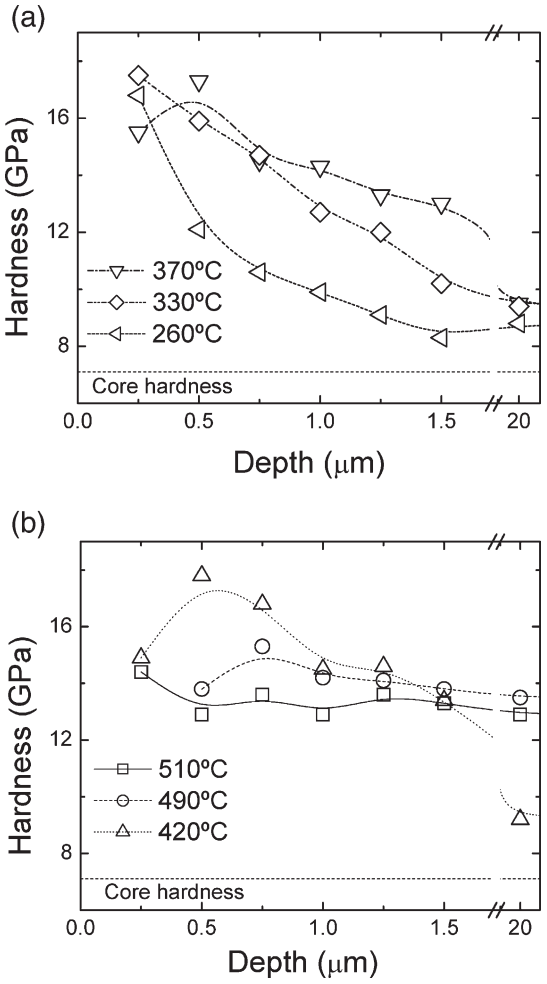

Fig. 2. Surface hardness for several treatment temperatures: (a) 260, 330 and 370 °C; (b) 420, 490 and 510 °C. Observe the axis break.

process temperatures (490 and 510 °C), the diffusion is fast enough to cause a nitrogen depletion concentration at the surface. Consequently, the γ′ phase (expanded fcc due to interstitial nitrogen) emerges and at 510 °C process temperature it is as intense as the peak corresponding to the ε-phase. We note that the Cu K_α radiation in the Bragg–Brentano geometry probes up to ~1.4 μm material depths. Therefore, the structures identified in Fig. 3(a) are correlated with depth hardness reported in Fig. 2. On the other hand, the GID measurements reported in Fig. 3 (b), obtained at 0.5° incident angle, probe a characteristic depth of ≤ 0.03 μm. Therefore, the information extracted from these diffractograms must be correlated only with the hardness data < 0.5 μm (Fig. 2) [24].

As suggested by the high surface frontal hardness values, the surface nitrogen concentration is relatively high in samples obtained even at the lower process temperatures (Fig. 2(a)). Indeed, the formation of a nitrogen-rich iron nitride compound is confirmed at 260 °C by the GID data. From Fig. 2(b), one can also conclude that, at 330 °C, a composed ε+α layer is formed, i.e., at depth ≤ 0.5 μm a compound ε layer is formed followed by a α phase diffusion layer. We stress the lack of evidence of an intermediary γ′ phase at 260 and 330 °C nitriding temperatures (Fig. 2(a)) [19].

The narrowing of the full-width at the half-maximum (FWHM) observed in the diffraction peaks indicates less disorder on increasing process temperatures (Fig. 3(a) and (b)). This is due to the fact that the higher temperature augments nitrogen mobility, promoting the formation of crystalline phases. On the other hand, at lower process temperatures, nitrogen accumulates on the top of the sample, inducing disorder and stressing the network. Finally, as remarked above, the ε and ε+γ′ crystalline phases are compatible with the relatively high hardness obtained in the samples.

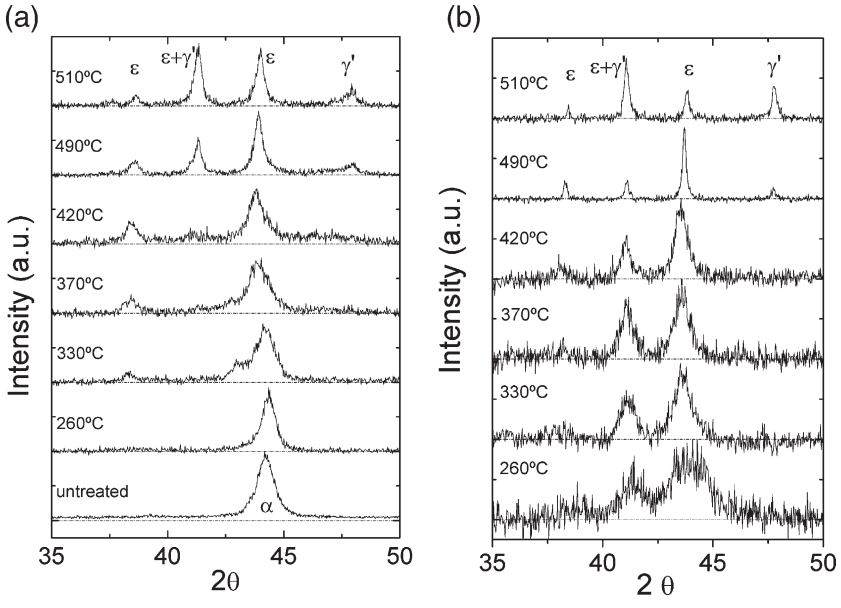

Fig. 3. (a) Bragg–Brentano X-ray diffraction of the studied samples. The process temperature is indicated. The phases α (body cubic centered, bcc), ε (hexagonal close packed, hcp, $Fe_{2-3}N$), and γ′ (expanded face cubic centered, fcc, due to interstitial N) are indicated; (b) diffractograms obtained by GID of the studied samples showing the peaks corresponding to the outermost surface layer.

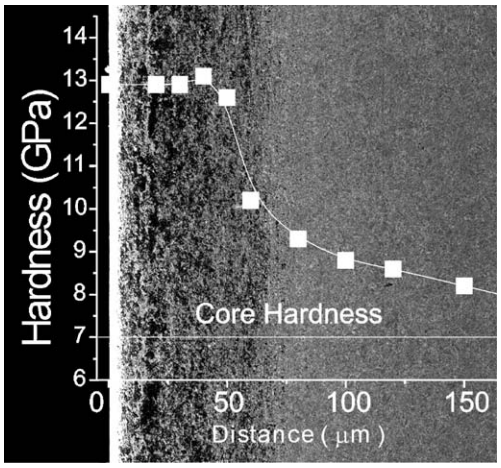

Fig. 4. SEM cross-section of the sample nitrided at 510 °C showing the chemically etched zone. The hardness profile is also superimposed.

3.3. Microstructure of the nitrided layer

Fig. 4 shows the in-depth profile hardness of samples treated at 510 °C superimposed on the SEM micrograph. The chemically attacked region revealing the nitrided layer is clearly observed.

Fig. 5(a) and (b) shows the SEM cross-section picture in the backscattered electrons signal mode of the same sample displayed in Fig. 4. The presence of metallic nitride precipitation and a ~6 μm thick white layer are clearly observed (Fig. 5(a)). The use of higher electron beam energy enhances the presence of precipitates (black and white dots, Fig. 5(b)). Similar features to those described for the sample processed at 510 °C are observed in samples treated at 490 °C. In Fig. 5(a) a line shows the transition between high and medium hardness as determined by Fig. 1. It is noted that there is a clear microstructure chance from one zone to the other one (Figs. 5 (a) and 4).

An estimate precipitate concentration is displayed in the right part of Fig. 5(b). We note that precipitate concentration vanishes monotonically while the hardness profile is almost constant up to 50 μm, decreasing afterward. This observation suggests that hardness has no simple dependence on precipitates of metallic nitrides.

Fig. 6(a) and (b) shows a cross-section micrograph of the sample nitrided at 370 and 420 °C, respectively. Fig. 6(a) shows a ~3–4 μm thick diffusion layer followed by a layer containing relative high nitrogen concentration at the grain boundary (dark region) and few precipitates randomly distributed (white dots) [25]. We remark that the darker region at

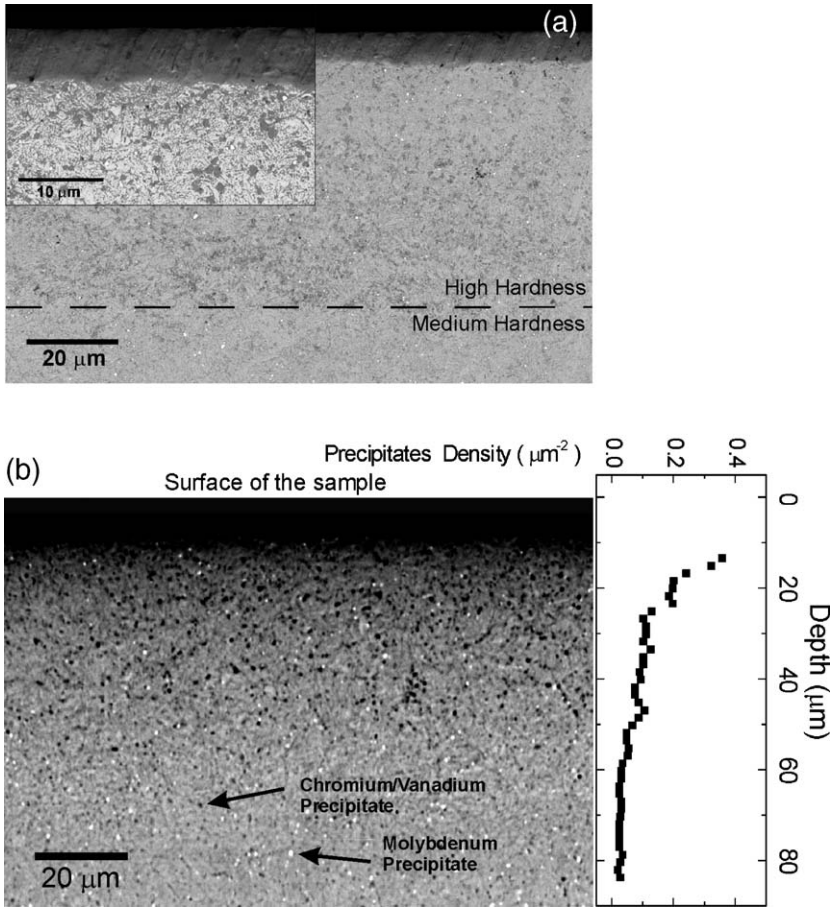

Fig. 5. SEM cross-section of sample displayed in Fig. 4. (a) Backscatter mode. The white layer (top gray shadow) and the region of nitrides precipitation (disperse gray spots) are clearly distinguished; (b) higher electron beam energies show chromium and vanadium rich precipitates (black dots). Right: The precipitates density profile is shown.

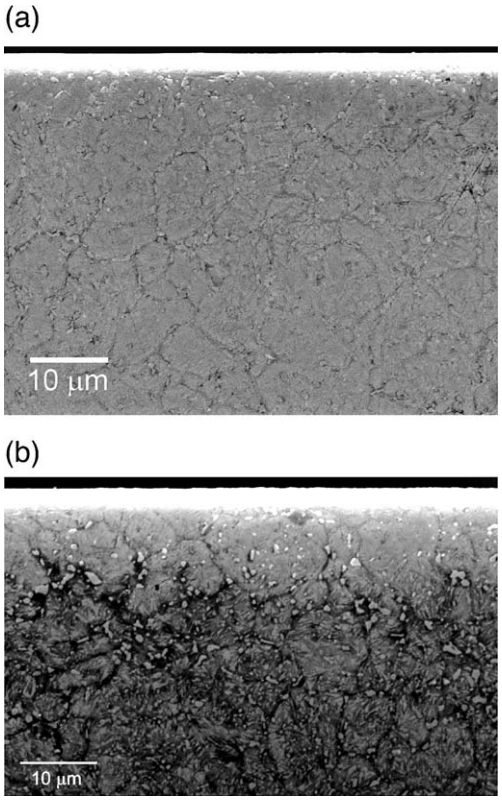

Fig. 6. (a) Micrograph of sample processed at 370 °C. The dark regions at the boundary grains show the presence of nitrogen. The bright white region at the picture top is an artifact due to edge effects; (b) SEM image showing the structures of a sample nitrided at 420 °C. The bright top region is an artifact due to edge effects.

the grain boundary indicates that diffusion takes place along these paths. Therefore, the low temperature processes have two consequences: a) reduction of the mobility of alloy elements preventing nitride precipitations; and b) enhancing free nitrogen at the grain boundaries, privileging this diffusion path.

The energy dispersive spectrometry (EDS) experiments provide a qualitative chemical material composition of the observed precipitates. The analysis shows that the darker small grains are vanadium and chromium rich regions (Fig. 5). Moreover, the white spots observed in Fig. 5 suggest higher local concentrations of molybdenum, a heavier atomic mass element. While most of the molybdenum seems to be already precipitated on carbide form, chromium/vanadium precipitates show great dependency on nitrogen content and process temperature. Indeed, higher magnification SEM micrographs (not shown) allow resolving changes on precipitates size and concentration. Table 2 summarizes the precipitate concentrations obtained near the surface and 80 μm depth for the sample treated at 510 °C. We call attention, however, that care must be taken in the interpretation of these pictures since the images were obtained from a bulk cross-section sample. A more correct procedure demands the use of a thin foil of known thickness material.

For the low temperatures process, the hardness depth profiles and the SEM analysis of microstructure show the presence

Table 2
Apparent size and density of precipitates in the pulsed plasma nitrided sample at 510 °C

Position	Density (precipitates/μm^2)	Diameter (μm)
Near the surface	~0.3	~0.8
In the depth of 80 μm	~0.03	~0.4

of a hard material at the outmost layers, i.e., a hard material is formed due to the relatively high nitrogen concentration. The contiguous region shows a difference between the content of nitrogen in bulk and that at the grain boundary (determined by Scanning Auger Microscopy). Finally, nitrogen concentration vanishes and the hardness goes to the bulk value.

3.4. The kinetics of the diffusion process

As remarked in the introduction, the material hardness scales fairly well to nitrogen concentration [12]. Therefore, a characteristic nitrogen diffusion length λ can be estimated from Figs. 1 and 2 at the onset, where the hardness falls from typical values of iron nitrides materials to those of the core values, i.e., where the first derivative is maximum. We remark that this mean length agrees very well with the diffusion thickness estimated from SEM micrographs, where the microstructure of the nitrided layer changes suddenly as the hardness curves.

From the Fick second law and assuming a constant concentration of nitrogen at the material surface during the nitriding diffusion process, follows $x^2/Dt=k_1$. Here x is the depth coordinated, D is the diffusion coefficient, t is the diffusion time, and k_1 is a concentration dependent constant [26]. Considering that $D=D_0\exp(-E_a/kT)$, where D_0 is constant, k is the Boltzman constant, E_a is the diffusion process activation energy, and T is the absolute temperature. Therefore, assuming equal diffusion times t, the characteristic diffusion length λ becomes:

$$\lambda = \lambda_0 \exp(-E_a/2kT). \quad (1)$$

Fig. 7 shows λ as a function of temperature. The plot confirms that the phenomenon follows the Arrenius type law, Eq. (1). The characteristic depth λ corresponding to the studied

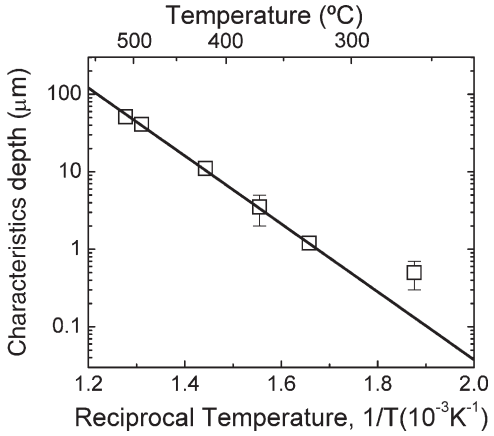

Fig. 7. Characteristic nitrogen diffusion depth λ as a function of temperature, T.

sample obtained at the lowest temperature, however, does not fit the exponential law well. This is caused by stress-induced hardness increase during the polishing. From Fig. 7, the activation energy was determined as $E_a = (165 \pm 10)$ kJ/mol. This value is higher than those reported by other authors in the ε and γ′ phases (~80 kJ/mol) [27–29]. This might be due to the alloying elements acting as nitrogen traps, increasing the activation energy of the process. Indeed, in stainless steel, where alloying elements limit nitrogen diffusion, higher activation energies have been reported [30,31].

4. Conclusion

The hardness and structural properties of AISI H13 tool steel treated by plasma pulsed nitriding at several temperatures are reported. The analysis of the hardness profile curves confirms the temperature activation diffusion of nitrogen. The relatively high activation energy obtained (165 ± 10 kJ/mol) suggests a complex diffusion mechanism involving the precipitation of alloying nitrides observed by SEM studies. At relatively lower process temperatures, a top layer (ε-phase) is formed. Underneath follows a region where nitrogen is mainly distributed at the grain boundary. At intermediate process temperatures (< 420 °C), nitrogen promotes metallic nitride precipitation at grain boundaries, moderately increasing the material hardness. Finally, at relatively higher process temperatures, nitrogen diffuses in the grains. Therefore, metallic nitrides are formed inside the grains, giving an important increasing hardness.

Acknowledgements

This work is part of the PhD thesis of L. F. Zagonel. The authors are indebted to D. Ugarte for the SEM measurements and to E. Mittemeijer for the critical reading of the manuscript. This work was partially sponsored by FAPESP, project # 97/12069-0. L. F. Zagonel and C. A. Figueroa are FAPESP fellows. F. Alvarez is CNPq fellow. The electron microscopy work was performed with the JSM-5900LV microscope of the LME/LNLS, Campinas, SP, Brazil.

References

[1] T. Czerwiec, H. Michel, E. Bergmann, Surf. Coat. Technol. 108 (1998) 182.
[2] M.K. Lei, Z.L. Zhang, T.C. Ma, Surf. Coat. Technol. 131 (2000) 317.
[3] M. Uma Devi, O.N. Mohanty, Surf. Coat. Technol 107 (1998) 55.
[4] J.C.A. Batista, M.C. Joseph, G. Pintaúde, A. Sinatora, C. Godoy, A. Matthews, Surf. Coat. Technol. 174 (2003) 891.
[5] A. Sokolowska, J. Rudnicki, P. Beer, L. Maldzinski, J. Tacikowski, J. Baszkiewicz, Surf. Coat. Technol. 142 (2001) 1040.
[6] M.K. Lei, Z.L. Zhang, Surf. Coat. Technol. 91 (1997) 25.
[7] L. Marot, L. Pichon, M. Drouet, A. Straboni, Mater. Lett. 44 (2000) 35.
[8] M.K. Lei, J. Mater. Sci. 34 (1999) 5975.
[9] B. Larisch, U. Bruxky, H.-J. Spies, Surf. Coat. Technol. 116 (1999) 205.
[10] Y. Sun, T. Bell, Surf. Eng. 19 (2003) 331.
[11] M.P. Fewell, J.M. Priest, M.J. Baldwin, G.A. Collins, K.T. Short, Surf. Coat. Technol. 131 (2000) 284.
[12] E.A. Ochoa, C.A. Figueroa, F. Alvarez, Surf. Coat. Technol. 200 (2005) 2165.
[13] I. Alphonsa, A. Chainani, P.M. Raole, B. Ganguli, P.I. John, Surf. Coat. Technol. 150 (2002) 263.
[14] M. Sennour, C. Jacq, C. Esnouf, J. Mater. Sci. 39 (2004) 4533.
[15] L.H. Corredor, B. Chornik, K. Ishizaki, Scr. Metall. 15 (1981) 195.
[16] W.C. Oliver, G.M. Pharr, J. Mater. Res. 7 (1992) 1564.
[17] W.C. Oliver, G.M. Pharr, J. Mater. Res. 19 (2004) 3.
[18] L. Ming-Kai, W. Xing-Jun, Chin. Phys. Lett. 19 (11) (2002) 1721.
[19] S. Malinov, A.J. Böttger, E.J. Mittemeijer, M.I. Pekelharing, M.A.J. Somers, Metall. Mater. Trans., A Phys. Metall. Mater. Sci. 32, 59 (2001).
[20] G.A. Collins, R. Hutching, J. Tendys, Surf. Coat. Technol. 59 (1993) 267.
[21] W.L. Li, Y. Sun, W.D. Fei, Appl. Surf. Sci. 187 (2002) 192.
[22] T. Liapina, A. Leineweber, E.J. Mittemeijer, W. Kockelmann, Acta Mater. 52 (2004) 173.
[23] H. Jacobs, D. Rechenbach, U. Zachwieja, J. Alloys Compd. 227 (1995) 10.
[24] J.A.-N., Des McMorrow, Elements of Modern X-ray Physics, John Wiley and Sons, Inc., NY, 2000.
[25] S. Mändl, E. Richter, R. Günzel, W. Möller, Nucl. Instrum. Methods B 148 (1999) 846.
[26] See for instance. W.D. Callister, Materials Science and Engineering. An Introduction, Fifth edition, John Wiley and Sons, Inc., NY, 1999.
[27] T. Bell, Y. Sun, Mater. Sci. Eng., A Struct. Mater.: Prop. Microstruct. Process. 224 (1997) 33.
[28] T. Belmonte, M. Gouné, H. Michel, Mater. Sci. Eng., A Struct. Mater.: Prop. Microstruct. Process. 302 (2001) 246.
[29] K. Ozbaysal, O.T. Inal, A.D. Romig Jr., Mater. Sci. Eng. 78 (1996) 179.
[30] M. Berg, C.V. Budtz-Jørgensen, H. Reitz, K.O. Schweitz, J. Chevallier, P. Kringhøj, J. Bøttinger, Surf. Coat. Technol. 124 (2000) 25.
[31] C.E. Pinedo, W.A. Monteiro, Surf. Coat. Technol. 179 (2004) 119.